Precision Engineering 85 (2024) 40–47

Contents lists available at ScienceDirect

Precision Engineering

journal homepage: www.elsevier.com/locate/precision

Surface determination algorithm for accurate XCT bidirectional length measurements

Xiuyuan Yang [a,b], Wenjuan Sun [b,**], Claudiu L. Giusca [a,*]

[a] Surface Engineering and Precision Centre, Cranfield University, Cranfield, Bedfordshire MK430AL, United Kingdom
[b] Engineering Department, National Physical Laboratory, Hampton Road, Teddington TW11 0LW, United Kingdom

ARTICLE INFO

Handling Editor: Dr. S Ludwick

ABSTRACT

Surface determination plays an important role in XCT bi-directional length measurement, however, its effect on the measurement results is often overlooked or hidden by other error sources. Most of the published research in dimensional field used the Canny algorithm or the surface determination module in VGStudio. Both of them require input from the operator that can also affect the accuracy of the measurements. Alternatively, the marker-controlled watershed (MCW) algorithm has been proven to avoid the latter issue, however, there is no systematic study that evaluated the surface determination algorithm's effect on the accuracy of bi-directional length measurements. In this study a two-sphere reference sample was measured using an XCT scanner and, with the aid of simulations, the effect of the three surface determination methods on bi-directional length measurements was comprehensively studied.

The results show that in the presence of 'streak' artefacts, a beam hardening error, if the operator does not set parameters appropriately, Canny and VGStudio implementations lead to either loss of surface or large errors, whereas MCW avoids this issue demonstrating its process automation ability. Nevertheless, with voxel calibration, beam hardening correction and data manipulation, MCW and Canny algorithms enable accurate sphere radius measurements (bi-directional measurements), comparable to the accuracy of an industrial tactile coordinate measuring machine.

1. Introduction

X-ray computed tomography (XCT) is a non-destructive three-dimensional (3D) measurement technique used in industry to evaluate components with complex geometries and out of site or internal features [1–5]. The lack of international measurement standards able to provide prescriptive guidelines for the use of XCT as a traceable dimensional measurement tool [6] restricts the industry implementation of XCT as a dimensional measurement tool. In an attempt to develop such guidelines, traceability studies [5,7], reviews [8–14], and interlaboratory comparisons [15,16] have been published in recent years, mostly covering the X-ray source [17,18], reconstruction [19], detector [20], comparison with traceable instruments, such as coordinate measuring machines (CMM) [7,16,21–25], and using smooth reference samples [6, 15,26,27] that evaluate the overall ability of XCT to measure the shape and form of components. Nevertheless, most of the published work overlooked the influence of surface determination algorithms (SDA) [28] on bi-directional length measurements [16,29–32]. The role of SDAs is to find, often with sub-voxel resolution, the boundary situated in the transition area between the background and the object, *i.e.* the surface.

Despite the importance of the surface determination process, the commercial software commonly used in industry and research does not allow to evaluate the magnitude of the effect of different error sources on the length measurements – *i.e.*, commercial SDA is regarded as a black box – hindering the development of complete measurement models. For example, a typical error is beam hardening caused by the reconstruction process, which assumes a linear attenuation of the X rays as they pass through the material [33]. Most of X-ray sources are polychromatic; hence, their attenuation coefficient is both energy and material-dependent, thus not linear. Beam hardening leads to material dilation [34–40], which can seriously affect the SDA output [13,41–43].

Previously, Canny, marker-controlled watershed (MCW) and the surface determination module available VGStudio Max (VG), a

* Corresponding author.
** Corresponding author.
E-mail addresses: wenjuan.sun@npl.co.uk (W. Sun), c.giusca@cranfield.ac.uk (C.L. Giusca).

https://doi.org/10.1016/j.precisioneng.2023.09.003
Received 1 February 2023; Received in revised form 4 September 2023; Accepted 5 September 2023
Available online 18 September 2023

commercial software, were reviewed [44] and it has been demonstrated that, for the 2D case, MCW can reduce the SDA errors and eliminate the errors associated with the operator's input [28]. However, the significant size of the XCT volumetric data leads to additional challenges, such as the implementation of algorithms, computer memory and processing time. For example, the interpolation to obtain sub-voxel location of the surface, can reach 1 TB of data size for a volumetric data of 500 × 500 × 500, when dividing a unit voxel length to 10 with double precision numerical resolution. Hence, another approach to obtain the surface with sub-voxel refinement is required for volumetric data processing.

The aim of this work is to evaluate the accuracy of Canny, VG and MCW in the 3D XCT sphere radius measurement context, a type of bi-directional length measurement. The next section details the methodology adopted during the investigation, which includes details about the SDAs trials, measurements and simulations used to optimise the SDAs output. The trials results and detailed discussions are presented in the third and fourth sections, respectively. Finally, the last section includes the summary of the main findings and conclusions.

2. Methodology

Canny implementation [7,45–55] – Canny uses a pair of normalised thresholds, *low* and *high*, to select the local maxima computed from the gradient image. The *hard edge* comprises of the maxima larger than the *high* threshold. The maxima smaller than the *low* threshold are discarded along with the maxima seating between the *high* and *low* threshold that is not connected to the *hard edge*. Canny threshold values used in previous research are often missing, impeding data reproducibility and the evaluation of the associated errors. To overcome these issues, nine trials with different thresholds are reported here, see Table 1: C1 to C5 are characterised by a small difference between *low* and *high* threshold values, whereas C6 to C9 have larger *high-low* threshold gaps.

VG implementation – VG employs a surface determination method based on the Steinbeis [56] algorithm, which provides an initial surface using a global threshold value (ISO50 [57]) within two regions manually selected, one for the background and one for material, then derives the final position of the surface by looking for the greatest gradient of the grey value within a pre-set search distance [58]. The effect of VG threshold and the search distance selection were rarely documented. To investigate the influence of these inputs, VG algorithm was tested using a Taguchi plan [59–61], where four commonly used settings in VG were considered: voxel search distance, background and material selection, and 'iterative surface determination', as shown in Table 2. For background and material selection, the term 'away from edge' indicates that the region of interest was selected at least 100 voxels away from the edge and 'close to edge' was within 100 voxels from the edge.

MCW implementation [28] - MCW first creates foreground and background markers with closing and erosion using the cubic structuring element built in MATLAB `strel('cube',num)`, where **num** is the structuring element size), followed by gradient and geodesic transformation, watershed transformation and voxel refinement, which are described in Ref. [28]. Four trials of MCW are listed in Table 3. The initial thresholds were estimated either automatically (ISO50) or manually (threshold corresponding to material peak).

Table 1
The threshold settings for the Canny algorithm.

Trials	Low threshold	High threshold
C1	0.0	0.2
C2	0.2	0.4
C3	0.4	0.6
C4	0.6	0.8
C5	0.8	1.0
C6	0.1	0.6
C7	0.3	0.9
C8	0.1	0.4
C9	0.5	0.9

Table 2
Taguchi orthogonal array for VG.

Trials	Voxel search distance/voxel	Background selection	Material selection	Iterative surface determination
VG1	2	Away from edge	Away from edge	on
VG2	2	Close to edge	Close to edge	off
VG3	4	Away from edge	Away from edge	off
VG4	4	Close to edge	Close to edge	on
VG5	10	Away from edge	Close to edge	on
VG6	10	Close to edge	Away from edge	off
VG7	20	Away from edge	Close to edge	off
VG8	20	Close to edge	Away from edge	on

Table 3
Parameter setting for 3D MCW algorithm.

Trials	Initial estimate	Cubic structuring element size (voxels)
MCW1	Automated	20
MCW2	Automated	40
MCW3	Manual	20
MCW4	Manual	40

Reference material: To evaluate the influence of SDAs on the XCT bi-directional length measurements, this work used a combination of XCT measurements and equivalent simulations of a physical reference sample (RS) and of a virtual reference (VR), respectively (see Fig. 1). The simulations were used to unpick the effect of measurement noise, beam hardening and beam hardening correction on the SDAs, which is not possible to separate from actual measurements.

The RS was a calibrated two-sphere titanium sample (density of 4.5 g/cm^3), placed on a supporting aluminium platform (density of 2.7 g/cm^3), providing both centre-to-centre (uni-directional) and spheres radii (bi-directional) reference length measurements [7,45–55]. Dimensional measurements were made using an F25 Coordinate Measuring Machine (CMM) fitted with a 0.3 mm diameter ruby ball tip. Measurements were made in the temperature range 20 °C ± 0.1 °C. The upper hemisphere of each sphere was contacted in a regular pattern of one hundred and fifty-six points, with a Gaussian substitute sphere fitted to the points. The RS calibration results, and their associated expanded uncertainties, are.

- Sphere 1 radius (2.540 8 ± 0.000 4) mm
- Sphere 2 radius (2.540 9 ± 0.000 4) mm
- Centre-to-centre distance (7.965 6 ± 0.000 4) mm

The expanded uncertainty is based on a standard uncertainty multiplied by a coverage factor k = 2.14, providing a confidence

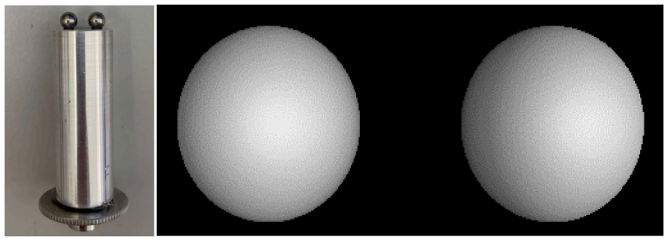

Fig. 1. Reference sample (RS) left and virtual reference (VR) right.

probability of approximately 95%.

The distance between the centres of the two spheres were used to calibrate the voxel size, which is essential in the adjustment and calibration of the sensitivity of the scales of the XCT [43,62,63]. The centre-to-centre measurements minimise the effect of the errors introduced by the SDA and material effects, such as beam hardening [43,62,63]. Note that in traditional tactile coordinate metrology uni- and bi-directional are point-to-point measurements, whereas here the sphere centre distance and the sphere diameter are considered.

The VR was realised by a simplified CAD model of the RS, having the same dimensional characteristics and material properties. The VR was generated using aRTist V2.1.0 [64]. The mesh surface of the VR consists of a set of 556,110 triangles, which is a compromise of computational cost and accuracy for the following simulation purposes. A comprehensive review of 3D mesh surfaces is provided in Ref. [65].

XCT measurements: The RS was measured three times by a Nikon XT H 225 M, fitted with a four-megapixel flat panel detector and using the following nominal scanning parameters: voltage 60 kV, current 100 μA, number of projections 3142, magnification 8, voxel size 25 μm, filter 0.5 mm Cu.

XCT Simulations: aRTist V2.1.0 was used to simulate the XCT measurement of the VR in various conditions, which are presented in Table 4. The simulations replicated the key experiments scanning parameters used in the measurements of the RS using a Nikon XT H 225 M instrument, including noise (level of 1.05). Simulation 1 represented an ideal situation and was used to benchmark the other four simulations. The simulations helped to investigate beam hardening and noise effects that could not be derived from the measurement of RS. The scattering, focal spot size effects were evaluated by comparing the measurement results and simulations, which did not account for these two error sources.

Data processing: The experimental and simulation projection images were used to generate volumetric data as follows.

- A shading correction was applied to the 2D measurement projections [2] and a field correction was applied to the 2D simulated projections [64].
- The beam hardening correction (BHC), based on the linearisation method [37], was applied in MATLAB 2019b to the experimental and simulated 2D projections corresponding to Simulation 4, to be able to compare the SDAs output with and without BHC.
- CTPro 3D Version XT 5.4 reconstruction software, developed by Nikon Metrology, was used to reconstruct volumetric data from the 2D projection images. (Note that because BHC was applied in MATLAB 2019b, the noise reduction and BHC available in CTPro 3D VersionXT 5.4 were disabled).
- The volume data, including the two spheres and excluding the supporting materials, consisting of 700 × 300 × 300 voxels, was exported in a '.vol' file format (246 MB) and used to evaluate SDAs.

Canny and MCW have been applied in MATLAB 2019b after a voxel refinement was performed with a window size of three voxels, as explained in Ref. [66].

The sphere radii estimates for each SDA trial were compared to the corresponding calibrated values. MCW and Canny sphere radii were calculated in MATLAB R2019b using a least square fitting algorithm [67]. The radii calculation for VG was performed using the sphere determination module available in VGStudio MAX 3.2.5 [68], in which the fit points were selected automatically with an error threshold of fitting points set at 0.15 mm and within two iterative processes, allowing a better comparison with the MATLAB results. The VG sphere determination module was used eight times to calculate the radii means and the associated standard deviations. The VG radius calculation was also performed using MATLAB R2019b least square fitting algorithm, and the results were found to be 50 nm different compared to sphere determination module available in VGStudio MAX, possibly due to the differences in the algorithms used to estimate the radius.

The radii were estimated using the XCT measurements of the portion of the spheres sitting above the holding material of the reference sample, which also coincided with the sphere portion measured during the RS calibration. As there was no holding material present in the XCT simulations, the sphere radii were evaluated using the whole sphere.

Table 4
Simulation conditions.

Simulation id	Spectrum type	Noise level set	Cu filter/mm
1	*Monochromatic*	0	0
2	*Polychromatic*	0	0
3	*Polychromatic*	1.05	0
4	*Polychromatic*	1.05	0.5

3. Results

Fig. 2 presents summary results of the SDA trials, *i.e.* sphere radius errors, implemented in simulations and, for indication only, one measurement of sphere 1 (note that a summary of measurement results is presented at the end of this section). Simulation 4 results with and without BHC correspond to the measurement results with and without BHC, respectively. Simulations 1 to 3 provide an indication of the effect of noise and polychromatic X-ray spectrum on the radii estimates. All SDAs were assessed using the same volumetric data; however, the Canny and MCW sphere interpolation method was different from the VG. VG radius calculations using the MATLAB 2019B sphere interpolation method, which are not shown in Fig. 2, lead 50 nm smaller mean radius errors across all VG results. The standard deviation associated with the residual of the Canny and MCW point cloud after sphere fitting was 2 μm, while standard deviation of VG data was 1 μm.

3.1. Summary of canny trials

C1 and C5 trials were found to be the most problematic. C1 was not able to discriminate between the edge of the spheres and the edge of the support material when applied on the XCT measurement of RS due to the low value of the high threshold (see Fig. 3 – C1). In contrast, C5 failed to return any surface (see Fig. 3 – C5) in the XCT measurement with BHC case and some of the simulations, as both thresholds were set too high.

Apart from C1 and C5, all other Canny trials successfully detected the surface of the RS and VR; measurement results with BHC yielded small radius errors. In addition, it was found that there was no significant difference between simulation 2 and 3, possibly because the noise only increased the dispersion of the surface point cloud and did not

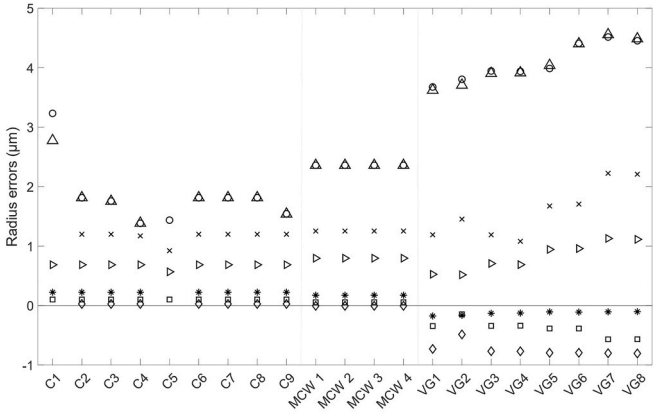

Fig. 2. Summary of SDA trials for both one measurement of sphere 1 and simulations.

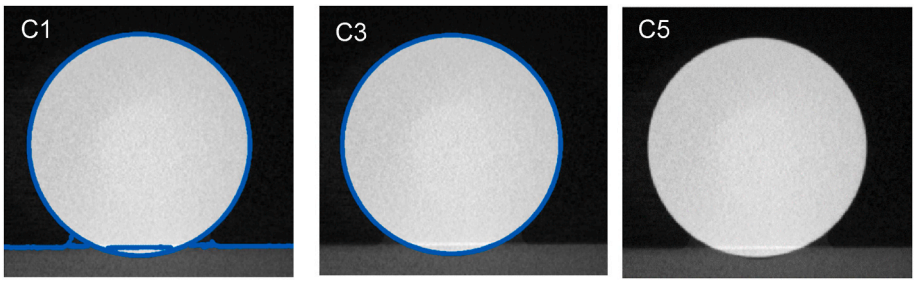

Fig. 3. Example of Canny results applied to the measured data with BHC.

contribute to the dilation or erosion of the spheres.

Without any filter or BHC (Simulation 2), a gradual increase of the lower threshold value in the Canny algorithm led to an increased loss of surface data around the streak artefacts, as shown in Fig. 4, resulting in a smaller radius deviation compared with other Canny threshold settings.

Loss of surface data did not occur in measurement after BHC. The measurement results were mirrored in simulation 4 with BHC where the streak artefacts were eliminated, and no gaps were found.

The best results were obtained in C4 trial.

3.2. Summary of VG trials

For both the measurement and simulations, the sensitivity of VG algorithm to the user-defined threshold decreased after applying BHC. For the measurement with BHC, VG2 provided the lowest magnitude error.

Without BHC, the increase in the search distance led to material dilation – see trials VG5 to VG8 and the low and high search distance led to up to 1 μm difference in radii, with lower error for the low search distance, highlighting that the beam hardening effect was a primary contributor to the bidirectional measurement errors.

Simulation 3 led to incorrect surface detection around streak artefact, see Fig. 5. Trials VG1 and VG3 had the background and material ROI away from the edge, such that the surface around the streak artefact was departing from the edge of the sphere. In VG2 and VG4 cases, background and material ROI were closer to the edge, but VG identified an additional boundary, which does not belong to the sphere. Only the increase in voxel search distance was able to effectively determine the boundary around the sphere (from VG5 to VG8). Nevertheless, radius calculation automatically disregarded the regions affected by large errors in VG1 to VG4, leading to lower radius values compared with the rest of the trials VG5 to VG8, in which the 'streak' affected zone was included in the radius calculation.

The best radius measurement results were obtained in VG4 trial.

Fig. 4. C3 surface result on Simulation 2 (marked as "O" in Fig. 2).

3.3. Summary of MCW trials

MCW successfully detected the surface in all cases and there were no differences for different MCW trials. When applied to simulations with BHC, MCW yielded relatively small radius errors.

Fig. 6 is the surface result by MCW. By comparison with Fig. 4 (Canny) and Fig. 5 (VG), MCW trials had no problems when dealing with the 'streak' artefact.

Following SDAs trials, C4, MCW and VG4 were used to determine the spheres surface for all three XCT measurements. Fig. 7 presents the mean of the mean radius errors of the two spheres and their associated combined standard deviations of the mean.

4. Discussions

Fig. 8 presents the schematic methodology of the following discussions and illustrates the areas that have been covered previously by other researchers.

4.1. Measurements without BHC (x) vs measurements with BHC (⋄)

The difference between measurements with and without BHC recorded in VG4 case was (−9.5 ± 1.1) % of the voxel size (VS), demonstrating that beam hardening has a dilation effect, which corroborates with the results reported by Tan [37] (−12.8% of VS) performed with a Cu filter and BHC. The magnitude of this difference was marginally larger in Tan's case possibly because of different measurement conditions: power, magnification, material (steel), BHC (polynomial) and VG parameters (not specified in Ref. [37]). The polynomial BHC is known to 'over-correct' the data [37] when the magnitude of its coefficients is not appropriately optimised.

4.2. Polychromatic simulations without BHC (o) vs monochromatic (✳)

Lifton [69] (Material: Al, Cu filter, VS = 63.5 μm, cylinder measurement, VGStudio) found that the difference between monochromatic and polychromatic was −20% VS with VG while in this research was −16% VS, although for Canny and MCW the differences were −5.6% VS and −8.4% VS, respectively, which is likely to be caused by the 'cupping' effect [13,41–43].

The difference between VG and MCW/Canny can be attributed to errors that usually appear in the polychromatic XCT measurement of multiple adjacent objects [50], here for example the two adjacent spheres (see the two protruding parts on each sphere in Fig. 9). Under

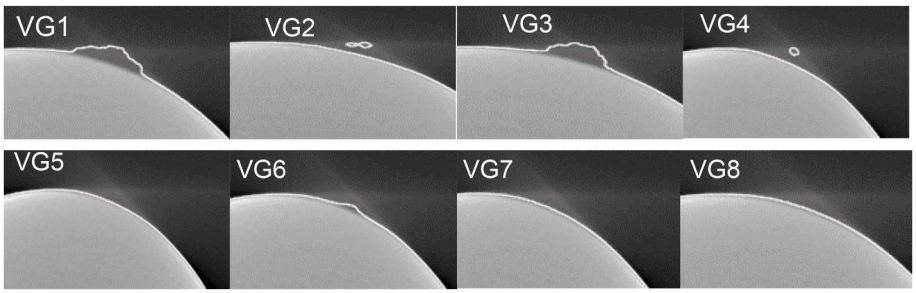

Fig. 5. VG trials for simulation 3.

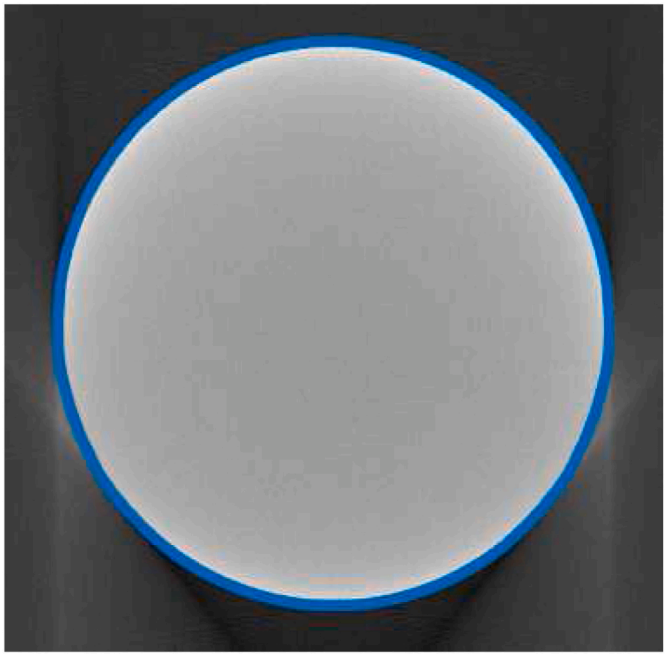

Fig. 6. The result of all MCW trials generated using MATLAB 2019b. (Measurement with copper filter, no BHC).

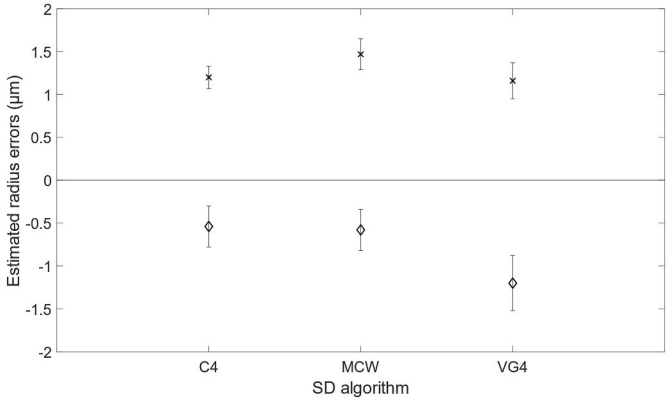

Fig. 7. Summary XCT results of three repeated measurements (mean radius errors and their associated standard deviations) using the optimised SDA: × Measurement – with copper filter – no BHC; ◊ Measurement – with copper filter – with BHC.

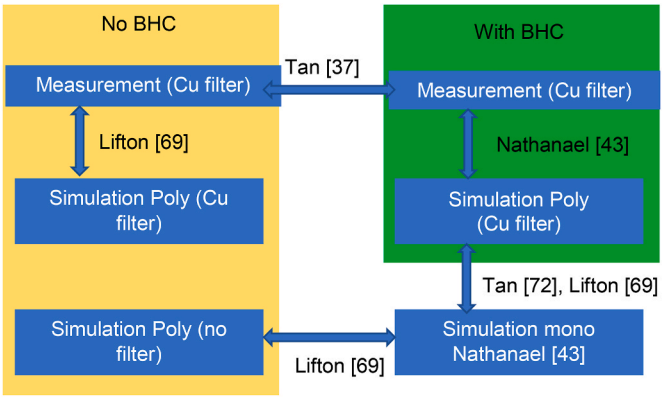

Fig. 8. The discussion comparison flowchart.

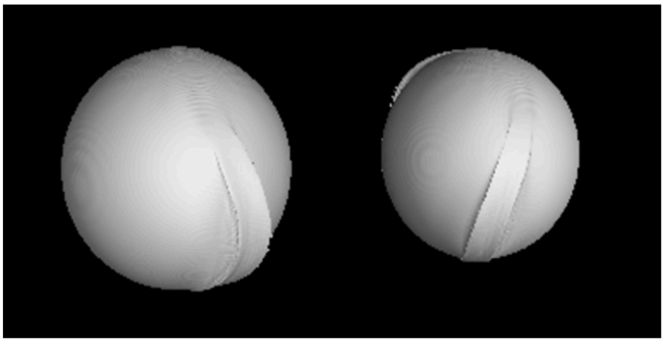

Fig. 9. Simulation 2 - polychromatic simulations reconstruction result.

the monochromatic condition, there were no such errors.

4.3. *Measurement without BHC (x) vs polychromatic simulation without BHC (▷)*

Without BHC, the radius measurement errors were consistently higher than their corresponding simulations (Simulation 4 without BHC), (1.5 ± 0.8) % VS for VG, (1.6 ± 0.5) % VS for Canny and (2.7 ± 0.7) % VS for MCW. In this work, the difference between the simulations and experiments without BHC is likely due to the effect of scattering [29,43] and the finite focal spot size [20,43,70,71] that lead to material dilation and were not included in simulations due to the complexity of the error model and computational cost. In addition, higher attenuation increases the contrast of the edge and therefore can also cause material dilation [41,43]. Lifton [69] (Cu filter, VS = 49 μm, VGStudio) reported a difference of 31.63% VS between measurements and simulation of an outer radius of a lower density cylinder, (aluminium), which was not found in this work. Lifton's difference between measurement and simulations were likely to be due to the improper voxel size calibration in

the experimental work.

4.4. Measurement with BHC (◇) vs simulation with BHC (□)

With BHC, the difference between measurement and simulations change sign and slightly increase in magnitude for Canny and MCW case and doubles in VG case, compared to without BHC results. Nathanael [43] reported a difference between measurement and simulation (material: steel, VS = 50 μm, Cu filter of 2 mm, VGStudio) of 8% VS, twice larger than the one observed here. The difference between Nathanael [43] and this work could be attributed to the difference in BHC implementation, voxel calibration, and material density.

4.5. Monochromatic (✳) vs simulation with BHC (□)

The monochromatic results should be nominally identical to polychromatic with BHC, assuming that BHC is able to entirely eliminate the beam hardening effect.

Tan's [72] study (material: steel, VS = 39 μm, Cu filter of 2 mm, VGStudio, BHC with different polynomial coefficients) reported radius errors ranging from (1.2–10) % VS between polychromatic with BHC and monochromatic simulations. Lifton [69] reported a radius difference of 12% VS for an Al sample and 24% VS for Ti sample In this study, VG4 recorded, 1% VS, for Ti. This shows that the component density is not a major contributor but rather the type of BHC and VG parameters selection is the major source of potential errors.

In monochromatic case, VG appears to erode the material. Nathanael [43] also used similar settings in VGStudio to the ones used in VG4 trial and concluded that the smoothing operation on the projection image before XCT reconstruction caused material erosion. However, in this study Canny and MCW show material dilation. Nevertheless, Canny and MCW used the least square fitting from MathWorks [67] to determine the sphere, while VG used its in-built iterative sphere determination algorithm. Unfortunately, VGStudio does not provide open access to the software, hence the hypotheses related to reconstruction erosion effect cannot be assumed just assessing the VGStudio results.

5. Conclusions

3D XCT measurements and simulations were conducted to evaluate the effect of SDA, noise and beam hardening on the accuracy of the radius measurement of a sphere, a bi-directional length measurement. In practice, surface determination is implemented with the help of a commercial software (VG) VGStudio or using Canny algorithm in MatLab. Both of these two surface determination implementations require input from the operator, which can lead to errors. MCW has been proposed as an alternative 2D SDA, because it does not need a specific operator input.

To examine and compare Canny, VG and MCW ability to provide accurate sphere radius measurements, all three SDAs were subject to different trials designed to find the optimal software setting parameters.

Canny trials were conducted to establish the optimal *low* and *high threshold* values and, apart from two extreme cases – *low threshold* too low or too high, the algorithm performed well in terms of radius errors. Nevertheless, the surface data around artefacts 'streak' artefact was lost without beam hardening correction.

VG trials showed a sensitivity to the *search distance* without beam hardening correction. An increase in the voxel search distance led to a sphere dilation. A small voxel search distance led to errors around the 'streak' artefact, but without loss of surface data.

MCW trials provided similar results in all trials, demonstrating that the algorithm implementation can be fully automated. In addition, MCW did not encounter issues around 'streak' artefacts - no data loss, no major errors.

This study shows that with proper scanning, calibration and data manipulation, such as Cu filter setup, beam hardening correction and SDA, XCT can provide accurate bi-directional length measurements. For example, Canny and MCW radius errors after beam hardening correction were found to be below 600 nm. VG errors were found to be twice as large, yet less than 5% of the voxel size. Unlike previously published work [43,69], the accuracy of the results was improved because the voxel size was calibrated using the same reference sample, *i.e.* XCT was used as a comparator.

As previously recorded in literature, without BHC, polychromatic X-rays lead to a dilation of the sphere [42]. Simulations showed that the VG radius difference between polychromatic and monochromatic beam was 16% of voxel size, close to Lifton's [69] work (20% of voxel size). Nevertheless, Canny and MCW corresponding differences were half of the VG difference.

In practice, with a polychromatic beam, the dilation effect can be mitigated with a Cu filter, but not sufficient, and an appropriate beam hardening correction algorithm has to be used to improve bi-directional length measurements. Even with the Cu filter and beam hardening correction, simulations show that there is a clear difference between the output of different SDAs, Canny and MCW results being situated closer to the simulated monochromatic response.

Previously it was hypothesised that the 3D reconstruction can lead to an erosion effect [43], the conclusion was based on VG analysis. Here, Canny and MCW led to a small dilation and VG to a small erosion in the monochromatic and polychromatic with Cu filter and BHC studies. However, all the experimental results after BHC indicate erosion, which indicate that there are other underlying errors affecting the measurement results, not simply the reconstruction.

Although, in this work the measurement was limited to a Ti sample, by comparing the results with previous findings in Ref. [72], it was found that beam hardening correction was the main source of errors.

Overall, all three surface determination implementations tested showed good sphere radius measurements (bi-directional measurements) performance, however, Canny and MCW were found to be marginally better compared to VG. At the same time, Canny and VG appear to determine the surface with errors or gaps around the 'streak' artefacts. The magnitude of the errors reported here may change when measuring complex shapes and rough workpieces.

The MCW algorithm used in this study can be accessed through the Cranfield University repository (CORD) at: https://doi.org/10.17862/cranfield.rd.24160512.v1.

Author statement

Xiuyuan Yang: Conceptualisation, Methodology, Software, Validation, Investigation, Formal analysis, Writing-Original Draft, Visualization. Wenjuan Sun: Writing-Review & Editing, Supervision, Project administration, Funding acquisition, Conceptualisation, Methodology. Claudiu Giusca: Writing-Review & Editing, Supervision, Funding acquisition, Conceptualisation, Methodology.

Ethical approval

In the author's opinion, there are no ethical issues with the research presented in this paper. The authors confirm this manuscript has not been published elsewhere and is not under consideration by another journal.

Consent to participate

Not applicable.

Consent to publication

All authors consent to the publication of this paper.

Conflicts of interest

The authors declare no competing interests.

Open access

Declaration of interests

The authors declare that they have no known competing financial interests or personal relationships that could have appeared to influence the work reported in this paper.

Acknowledgements

This work was funded by the UK Government's Department for Business, Energy and Industrial Strategy (BEIS) through the UK's National Measurement System programmes and Centre for Doctoral Training (CDT) in Ultra Precision at Cranfield University which is supported by the RCUK via Grant No.: EP/K503241/1. The authors would like to thank Dr Allan Wilson (NPL) for the calibration of the reference sample.

References

[1] Kruth JP, Bartscher M, Carmignato S, Schmitt R, De Chiffre L, Weckenmann A. Computed tomography for dimensional metrology. CIRP Annals 2011;60:821–42.
[2] Zanini F, Carmignato S, Savio E, Affatato S. Uncertainty determination for X-ray computed tomography wear assessment of polyethylene hip joint prostheses. Precis Eng 2018;52:477–83.
[3] Villarraga-Gómez H, Morse EP, Smith ST. Assessing the effect of penetration length variations on dimensional measurements with X-ray computed tomography. Precis Eng 2023;79:146–63.
[4] Zwanenburg EA, Williams MA, Warnett JM. Performance testing of dimensional X-ray computed tomography systems. Precis Eng 2022;77:179–93.
[5] Zanini F, Carmignato S. Reference object for traceability establishment in X-ray computed tomography measurements of fiber length in fiber-reinforced polymeric materials. Precis Eng 2022;77:33–9.
[6] Villarraga-Gómez H, Herazo EL, Smith ST. X-ray computed tomography: from medical imaging to dimensional metrology. Precis Eng 2019;60:544–69.
[7] Sun W, Giusca C, Lou S, Yang X, Chen X, Fry T, et al. Establishment of X-ray computed tomography traceability for additively manufactured surface texture evaluation. Addit Manuf 2022;50:102558.
[8] Thompson A, Maskery I, Leach RK, Thompson A, Maskery I, Leach RK. X-ray computed tomography for additive manufacturing: a review. Meas Sci Technol 2016;27:072001.
[9] Townsend A, Senin N, Blunt L, Leach RK, Taylor JS. Surface texture metrology for metal additive manufacturing: a review. Precis Eng 2016;46:34–47.
[10] du Plessis A, Yadroitsava I, Yadroitsev I. Effects of defects on mechanical properties in metal additive manufacturing: a review focusing on X-ray tomography insights. Mater Des 2020;187:108385.
[11] Leach R, Haitjema H, Su R, Thompson A. Metrological characteristics for the calibration of surface topography measuring instruments: a review. Meas Sci Technol 2020;32:032001.
[12] Rodríguez-Sánchez Á, Thompson A, Körner L, Brierley N, Leach R. Review of the influence of noise in X-ray computed tomography measurement uncertainty. Precis Eng 2020;66:382–91.
[13] Villarraga-Gómez H, Thousand JD, Smith ST. Empirical approaches to uncertainty analysis of X-ray computed tomography measurements: a review with examples. Precis Eng 2020;64:249–68.
[14] Sun W, Symes DR, Brenner CM, Böhnel M, Brown S, Mavrogordato MN, et al. Review of high energy x-ray computed tomography for non-destructive dimensional metrology of large metallic advanced manufactured components. Rep Prog Phys 2022;85:016102.
[15] Carmignato S, Pierobon A, Savio E. CT audit–interlaboratory comparison of computed tomography systems for dimensional metrology. Final Report. Abridged version University of Padova; 2012.
[16] Townsend A, Racasan R, Leach R, Senin N, Thompson A, Ramsey A, et al. An interlaboratory comparison of X-ray computed tomography measurement for texture and dimensional characterisation of additively manufactured parts. Addit Manuf 2018;23:422–32.
[17] Sun W, Brown S, Woolliams P, McCarthy M, White J, Attallah M. Applications and systematic errors of X-ray computed tomography associated with dimensional metrology. In: 55th annual conference of the British institute of non-destructive testing, NDT 2016. Nottingham: British Institute of Non-Destructive Testing; 2016. p. 337–45.
[18] Flay N, Brown S, Sun W, Blumensath T, Su R. Effects of off-focal radiation on dimensional measurements in industrial cone-beam micro-focus X-ray computed tomography systems. Precis Eng 2020;66:472–81.
[19] Lohvithee M, Sun W, Chretien S, Soleimani M. Ant colony-based hyperparameter optimisation in total variation reconstruction in X-ray computed tomography. Sensors 2021;21:591.
[20] Sun W, Brown S, Flay N, McCarthy M, McBride J. A reference sample for investigating the stability of the imaging system of x-ray computed tomography. Meas Sci Technol 2016;27:085004.
[21] Leach R. The measurement of surface texture using stylus instruments. Measurement good practice guide no. 37. National Physical Laboratory; 2001.
[22] Leach RK, Giusca CL, Haitjema H, Evans C, Jiang X. Calibration and verification of areal surface texture measuring instruments. CIRP Annals 2015;64:797–813.
[23] Triantaphyllou A, Giusca CL, Macaulay GD, Roerig F, Hoebel M, Leach RK, et al. Surface texture measurement for additive manufacturing. Surf Topogr Metrol Prop 2015;3:024002.
[24] Townsend A, Pagani L, Blunt L, Scott PJ, Jiang X. Factors affecting the accuracy of areal surface texture data extraction from X-ray CT. CIRP Annals 2017;66:547–50.
[25] Townsend A, Pagani L, Scott P, Blunt L. Areal surface texture data extraction from X-ray computed tomography reconstructions of metal additively manufactured parts. Precis Eng 2017;48:254–64.
[26] Angel JAB, De Chiffre L. Inter laboratory comparison on industrial computed tomography. DTU Mechanical Engineering; 2013.
[27] Stolfi A, De Chiffre L. InteraqCT comparison on assemblies-final report. DTU: DTU Library; 2016.
[28] Yang X, Sun W, Giusca CL. An automated surface determination approach for computed tomography. NDT E Int 2022;131:102697.
[29] Lifton JJ, Carmignato S. Simulating the influence of scatter and beam hardening in dimensional computed tomography. Meas Sci Technol 2017;28:104001.
[30] Carmignato S, Dreossi D, Mancini L, Marinello F, Tromba G, Savio E. Testing of x-ray microtomography systems using a traceable geometrical standard. Meas Sci Technol 2009;20:084021.
[31] Müller P, Hiller J, Cantatore A, De Chiffre L. Investigation of measuring strategies in computed tomography. NEWTECH; 2011. p. 31–42. New Technologies in Manufacturing, 2011.
[32] Aloisi V, Carmignato S. Influence of surface roughness on X-ray computed tomography dimensional measurements of additive manufactured parts. Case Studies in Nondestructive Testing and Evaluation 2016;6:104–10.
[33] Lifton JJ, Malcolm AA, McBride JW. A simulation-based study on the influence of beam hardening in X-ray computed tomography for dimensional metrology. J X Ray Sci Technol 2015;23:65–82.
[34] Herman GT. Correction for beam hardening in computed tomography. Phys Med Biol 1979;24:81–106.
[35] Van Gompel G, Van Slambrouck K, Defrise M, Batenburg KJ, de Mey J, Sijbers J, et al. Iterative correction of beam hardening artifacts in CT. Med Phys 2011;38:S36–49.
[36] Dewulf W, Tan Y, Kiekens K. Sense and non-sense of beam hardening correction in CT metrology. CIRP Annals 2012;61:495–8.
[37] Tan Y, Kiekens K, Welkenhuyzen F, Kruth J-P, Dewulf W. Beam hardening correction and its influence on the measurement accuracy and repeatability for CT dimensional metrology applications. In: Conf. On industrial computed tomography; 2012. Wels, Austria.
[38] Rasoulpour N, Kamali-Asl A, Hemmati H. A new approach for beam hardening correction based on the local spectrum distributions. Nucl Instrum Methods Phys Res Sect A Accel Spectrom Detect Assoc Equip 2015;794:177–84.
[39] Kraemer A, Lanza G. Assessment of the measurement procedure for dimensional metrology with X-ray computed tomography. Procedia CIRP 2016;43:362–7.
[40] Kathryn M, Chiffre D, Stolfi A, Kathryn Thompson M, Carli L, De Chiffre L. Quantifying the contribution of post-processing in computed tomography measurement uncertainty. Procedia CIRP 2016;43:297–302.
[41] Sun W, Brown SB, Leach RK. An overview of industrial X-ray computed tomography. Queen's Printer and Controller of HMSO: National Physical Laboratory; 2012.
[42] Lifton JJ. The influence of scatter and beam hardening in X-ray computed tomography for dimensional metrology. University of Southampton, Engineering and the Environment; 2015. Doctoral Thesis: University of Southampton.
[43] Nathanael T. Erosion and dilation of edges in dimensional X-ray computed tomography images. PhD Thesis. Loughborough University; 2020.
[44] Reinhart C, Weg W. Industrial computer tomography - a universal inspection tool. 17th world conference on nondestructive testing. Shanghai, China: 17th World Conference on Nondestructive Testing; 2008.

[45] Müller P. Use of reference objects for correction of measuring errors in X-ray computed tomography. DTU Mechanical Engineering, Technical University of Denmark; 2010.
[46] Patterson BM, Hamilton CE. Dimensional standard for micro X-ray computed tomography. Anal Chem 2010;82:8537–43.
[47] Staude A. The influence of data filtering on dimensional measurements with CT. Durban, South Africa: WCNDT 2012; 2012.
[48] Sun Q, Zheng J, Li C. Improved watershed analysis for segmenting contacting particles of coarse granular soils in volumetric images. Powder Technol 2019;356:295–303.
[49] Fleßner M, Müller A, Helmecke E, Hausotte T. Automated detection of artefacts for computed tomography in dimensional metrology. Digital Industr. Radiol. Comput. Tomogr. 2015:1–8.
[50] Müller AM, Butzhammer L, Wohlgemuth F, Hausotte T. Automated evaluation of the surface point quality in dimensional X-ray computed tomography. TM - Tech Mess 2020;87:111–21.
[51] Ametova E, Ferrucci M, Chilingaryan S, Dewulf W. A computationally inexpensive model for estimating dimensional measurement uncertainty due to X-ray computed tomography instrument misalignments. Meas Sci Technol 2018;29:065007.
[52] Zanini F, Technology SCMSa, undefined. Two-spheres method for evaluating the metrological structural resolution in dimensional computed tomography. Meas Sci Technol 2017;28:114002.
[53] Levine ZH, Blattner TJ, Peskin AP, Pintar AL. Scatter corrections in X-ray computed tomography: a physics-based analysis. Journal of Research of National Institute of Standards and Technology; 2019. p. 124.
[54] Fei L, Dantan J-Y, Baudouin C, Du S. Calibration and uncertainty estimation of non-contact coordinate measurement systems based on Kriging models. Precis Eng 2019;57:16–29.
[55] Torralba M, Jiménez R, Yagüe-Fabra JA, Ontiveros S, Tosello G. Comparison of surface extraction techniques performance in computed tomography for 3D complex micro-geometry dimensional measurements. Int J Adv Des Manuf Technol 2018;97:441–53.
[56] Steinbeiß HP. Dimensionelles Messen mit Mikro-Computertomographie. Hieronymus; 2005.
[57] Lifton JJ, Liu T. Evaluation of the standard measurement uncertainty due to the ISO50 surface determination method for dimensional computed tomography. Precis Eng 2020;61:82–92.
[58] Thompson A, Senin N, Giusca C, Leach R. Topography of selectively laser melted surfaces: a comparison of different measurement methods. CIRP Annals 2017;66:543–6.
[59] Mistree F, Lautenschlager U, Erikstad SO, Allen JK. Simulation reduction using the Taguchi method. Integrated realization of engineered materials, products, and associated manufacturing processes. NASA; 1993.
[60] Schwaninger M, Hadjis A. Model building and validation: contributions of the Taguchi method. International System dynamics conference: international System dynamics conference. 1998. p. 1–13.
[61] Kumar R, Prajapati DDR, Singh S. Implementation of Taguchi methodology for defect reduction in manufacturing industry "A case study". Int J Ind Eng Res Dev 2011;2:1–14.
[62] Hiller J, Maisl M, Reindl LM. Physical characterization and performance evaluation of an x-ray micro-computed tomography system for dimensional metrology applications. Meas Sci Technol 2012;23:085404.
[63] Kiekens K. Contributions to performance verification and uncertainty determination of industrial computed tomography for dimensional metrology. PhD thesis: KU Leuven. KU Leuven; 2017.
[64] Bellon C, Jaenisch G-R. aRTist – analytical RT inspection simulation tool. In: International symposium on digital industrial radiology and computed tomography; 2007.
[65] Mangan AP, Whitaker RT. Partitioning 3D surface meshes using watershed segmentation. IEEE Trans Visual Comput Graph 1999;5:308–21.
[66] Yagüe-Fabra JA, Ontiveros S, Jiménez R, Chitchian S, Tosello G, Carmignato S. A 3D edge detection technique for surface extraction in computed tomography for dimensional metrology applications. CIRP Annals 2013;62:531–4.
[67] Jennings A. Sphere fit (least squared) MATLAB central file exchange. 2022.
[68] Graphics V. VGStudio MAX 3.0. Reference Manual 2016.
[69] Lifton JJ, Malcolm AA, McBride JW. An experimental study on the influence of scatter and beam hardening in x-ray CT for dimensional metrology. Meas Sci Technol 2016;27:015007.
[70] Flay N, Sun W, Brown S, Leach R, Blumensath T. Investigation of the focal spot drift in industrial cone-beam X-ray computed tomography. Digital industrial radiology and computed tomography. 2015. ghent, Belgium.
[71] Romanov AY. Measurement of the parameters of the focal spot of an x-ray tube using kumakhov optics. Meas Tech 2004;47:670–4.
[72] Tan Y, Kiekens K, Welkenhuyzen F, Angel J, De Chiffre L, Kruth J-P, et al. Simulation-aided investigation of beam hardening induced errors in CT dimensional metrology. Meas Sci Technol 2014;25:064014.

2023-09-23

Surface determination algorithm for accurate XCT bidirectional length measurements

Yang, Xiuyuan

Elsevier

Yang X, Sun W, Giusca CL. (2024) Surface determination algorithm for accurate XCT bidirectional length measurements, Precision Engineering, Volume 85, January 2024, pp. 40-47
https://doi.org/10.1016/j.precisioneng.2023.09.003